Int. J. Heat Mass Transfer. Vol. 35, No. 5, pp. 1059–1067, 1992
Printed in Great Britain

0017-9310/92 $5.00 + 0.00
Pergamon Press Ltd

# Rapid solidification following laser melting of pure metals—II. Study of pool and solidification characteristics

BISWAJIT BASU
Tata Research Development and Design Centre, 1, Mangaldas Road, Pune 411 011, India

and

A. W. DATE
Department of Mechanical Engineering, Indian Institute of Technology, Powai, Bombay 400 076, India

(*Received* 13 *June* 1990 *and in final form* 20 *May* 1991)

**Abstract**—Various solidification parameters, like solid/liquid temperature gradient, cooling rate, nature of latent heat release, and pool characteristics, i.e. rate of change of width, depth and maximum velocity of the pool, are studied for rapid solidification following laser melting of aluminium and steel. For a fixed laser radius (i.e. 2.0 mm), the studies are carried out with various beam power densities between $10^8$ and $10^9$ W m$^{-2}$. There is melting (i.e. 'post-melting') even after the laser is removed and the amount of post-melting is related to the amount of superheat of the pool. From the solid/liquid interface temperature gradient and the cooling rate, it is shown that the microstructure of the solidified material is very fine and the microstructure at the top of the pool is always finer than that at the bottom.

## 1. INTRODUCTION

THE PROPERTIES of a solidified material subsequent to laser melting are dependent on the microstructure which, in turn, is controlled by the solidification characteristics, namely, the velocity of the solidification front, the temperature gradient across the solid/liquid interface and the cooling rate [1]. Although the melting characteristics are independent of the solidification characteristics, the latter are integrally dependent on the former, i.e. melting time, flow field and temperature distribution at the end of melting. The thermal gradient across the solid/liquid interface, which is the rate controlling parameter for rapid solidification, is dependent on the melting characteristics.

Following laser melting, the liquid metal solidifies directionally on its own substrate. The substrate thus acts as a heat sink and the heat loss essentially takes place through the substrate along with a slow rate of heat loss (i.e. convective + radiative) from the free liquid surface. The rate of solidification subsequent to laser heating is therefore dependent on the fast rate of heat removal which consists of two parts—superheat removal and latent heat removal.

The rate of removal of the superheat determines how fast the solidification initiates and, once initiated, the solidification rate is controlled by the rate of latent heat extraction. Since the bulk of the heat is removed through the substrate, the temperature gradient at the solid/liquid interface determines the heat extraction rate. Hence, the rapid solidification during laser surface treatment is controlled by the following parameters:

- rate of loss of superheat;
- rate of loss of latent heat; and
- the temperature gradient at the solid/liquid interface.

These parameters govern the solid/liquid interface speed and the cooling rate and, in turn, the microstructure.

Besides the solidification characteristics described above, the pool characteristics are also important from the point of view of fundamental understanding, i.e. how does the front move radially and axially and what is the rate of decay of the flow field. The pool characteristics of interest are as follows:

- rate of decrease of the liquid width;
- rate of decrease of the liquid depth; and
- rate of decrease of the maximum velocity of the flow field in the liquid pool.

In all the earlier studies [2–7], detailed study of various pool and solidification characteristics in the presence of flow has not been carried out, although a similar study has been performed for arc welding [8]. In this paper, we present a comprehensive study of rapid solidification following laser surface melting using the model described by Basu and Date [9].

## 2. THE PARAMETERS STUDIED

The process parameters for the solidification study are the same as those reported in Basu and Date [9].

## NOMENCLATURE

| | |
|---|---|
| $A_I$ | area of the solid/liquid interface |
| $A_l$ | area of the liquid pool |
| $B_I$ | boundary heating factor, $qr_0C_p/k$ |
| $C_p$ | specific heat [J kg$^{-1}$ K$^{-1}$] |
| $f_l$ | liquid fraction |
| $k$ | thermal conductivity [W m$^{-1}$ K$^{-1}$] |
| $l_r$ | length along constant $z$ direction |
| $l_z$ | length along constant $r$ direction |
| $L$ | amount of latent heat release |
| $Ma$ | Marangoni number, $U_R r_0/\alpha$ |
| $Pr$ | Prandtl number, $\nu/\alpha$ |
| $q$ | laser heat flux [W m$^{-2}$] |
| $r_0$ | radius of the laser beam [m] |
| $r_{max}$ | width of the laser melted pool |
| $R_\sigma$ | surface tension Reynolds number, $U_R r_0/\nu$ |
| $Ste$ | Stefan number, $C_p(T_m-T_\infty)/\lambda$ |
| $t$ | time [s] |
| $T$ | amount of total heat released |
| $\lvert\dot{T}\rvert$ | cooling rate [K s$^{-1}$] |
| $\partial\bar{T}/\partial n\rvert_I$ | average solid/liquid temperature gradient [K mm$^{-1}$] |
| $U_R$ | characteristic velocity, $(d\sigma_s/dT)\cdot\lambda/\mu C_p$ [m s$^{-1}$] |
| $V_I$ | solid/liquid interface velocity |
| $V_{max}$ | maximum velocity of the fluid |
| $z_{max}$ | depth of the laser melted pool. |

Greek symbols

| | |
|---|---|
| $\alpha$ | thermal diffusivity [m$^2$ s$^{-1}$] |
| $\theta$ | non-dimensional temperature |
| $\lvert\dot{\theta}\rvert$ | non-dimensional cooling rate |
| $\lambda$ | latent heat of fusion [J kg$^{-1}$] |
| $\mu$ | dynamic viscosity [N m$^{-2}$ s$^{-1}$] |
| $\nu$ | kinematic viscosity [m$^2$ s$^{-1}$] |
| $\rho$ | density [kg m$^{-3}$] |
| $\tau$ | non-dimensional time |
| $\tau_{melt}$ | non-dimensional interaction time |
| $\phi$ | non-dimensional enthalpy. |

Subscripts

| | |
|---|---|
| bulk | bulk mean value |
| I | interface |
| l | liquid. |

Superscript

| | |
|---|---|
| * | dimensional value. |

The effect of the process parameters is studied with respect to the time rate of change of the following variables:

$$L/T = \frac{\text{rate of release of latent heat}}{\text{rate of release of total (superheat + latent) heat}}$$

$\theta_{bulk}$ the bulk mean temperature of the liquid which is also the superheat of the melt, $\partial\bar{\theta}/\partial n|_I$ the average temperature gradient at the interface, $r_{max}$ the melt width, $z_{max}$ the melt depth, and $V_{max}$ the maximum velocity of the fluid. The $(L/T)$ value is calculated as follows:

$$(L/T) = \left[\frac{\Sigma f_l\lambda|_{r,z}}{\Sigma C_p(T-T_m)+\Sigma f_l\lambda}\bigg|_I\right]_t^{t+\Delta t}$$

$$(L/T) = \left[\frac{\Sigma f_l}{\Sigma\theta_l+\Sigma f_l}\right]_\tau^{\tau+\Delta\tau}$$

where $f_l$ is the liquid fraction.

The bulk mean temperature of the liquid is determined as follows:

$$\theta_{bulk} = \frac{1}{A_l}\int_{A_l}\theta\,da.$$

The average temperature gradient is calculated on the basis of the interfacial area as follows:

$$\left.\frac{\partial\bar{\theta}}{\partial n}\right|_I = \frac{\Sigma\,\partial\theta/\partial r|_{\text{constant}\,r}\,r\,\Delta r+\Sigma\,\partial\theta/\partial z|_{\text{constant}\,z}\,r\,\Delta z}{A_I}$$

where $A_I$ is the area of the solid/liquid interface

$$A_I = \int_{l_z} r\,dr|_{\text{constant}\,z}+\int_{l_r} r\,dz|_{\text{constant}\,r}.$$

## 3. RESULTS AND DISCUSSION

### 3.1. *Study of solidification characteristics*

3.1.1. *Steel.* Figure 1 shows the transient variation of $(L/T)$, $\theta_{bulk}$ and $\partial\bar{\theta}/\partial n|_I$ for a beam of 2.0 mm radius and $4\times10^8$ W m$^{-2}$ power density with different melting times. Both $\theta_{bulk}$ and $\partial\bar{\theta}/\partial n|_I$ decrease with time and approach zero asymptotically; $(L/T)$ approaches unity. The important aspect of the rapid solidification process is to attain minimum superheat and also to ensure fast removal of the superheat. The time rate of change of both the parameters $(L/T)$ and $\theta_{bulk}$ shows how fast the superheat is being extracted out. From Fig. 1(a), it can be seen that the superheat is negligible at $\Delta\tau$ (i.e. $\tau-\tau_{melt}$) = 0.065 when the solidification is initiated at $\tau$ = 0.975. Beyond this time the solidification is mainly controlled by the latent heat removal. An interesting point can be seen by comparing $(L/T)$ variation for two different $\tau_{melt}$ values: 0.975 and 1.985. Figure 1(b) shows that $(L/T)$ is negative during a very small period at the initiation

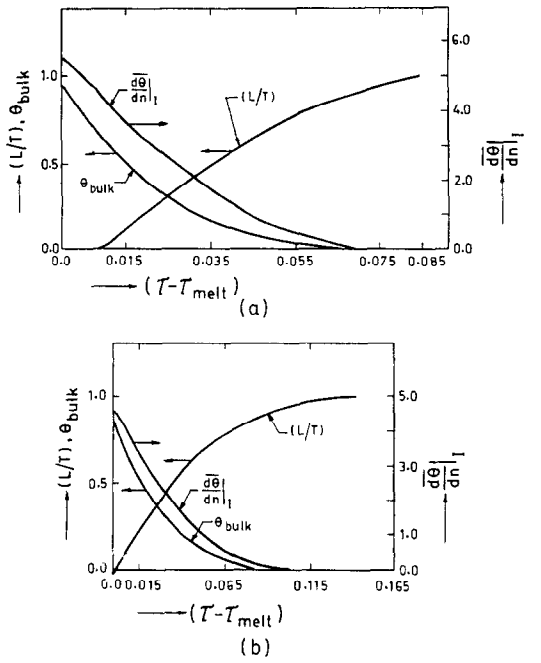


FIG. 1. The rate of change of the solidification characteristics, i.e. $(L/T)$, $\theta_{bulk}$ and $\partial\bar{\theta}/\partial n|_I$, for steel with a laser of $4.0 \times 10^8$ W m$^{-2}$ power density and 2.0 mm radius for various $\tau_{melt}$ values.

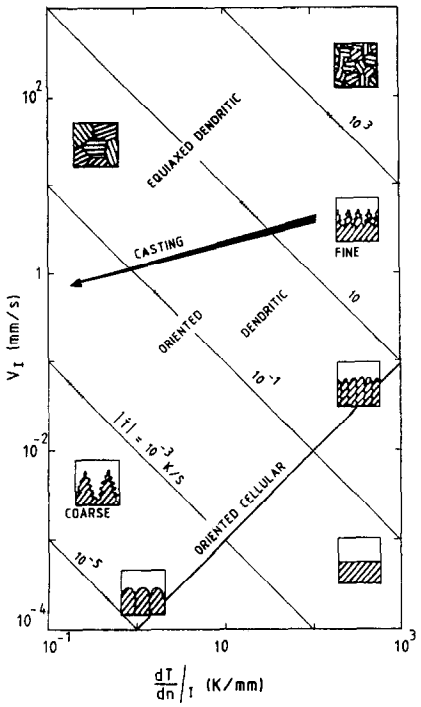


FIG. 2. Relationship between $\partial\bar{T}/\partial n|_I$, $V_I$ and cooling rate with microstructure of the solidified material [1].

of solidification. Though the input heat flux is removed, a small amount of melting takes place due to the superheat of the liquid pool itself; this melting can be designated as 'post-melting'. When $\tau_{melt}$ is small, this phenomenon is not seen due to the low energy (superheat) level of the pool. The average temperature gradient at the interface, $\partial\bar{\theta}/\partial n|_I$, varies in the same way as $\theta_{bulk}$. The maximum values of $\partial\bar{\theta}/\partial n|_I$ are 5.5 and 4.8 for $\tau_{melt} = 0.975$ and 1.985, respectively. When $\tau_{melt}$ is larger, the flow within the liquid pool is more vigorous, resulting in better mixing and subsequently lowering the average temperature gradient. In dimensional form, the values of $\partial\bar{T}/\partial n|_I$ are 1270.0 and 1109.0 K mm$^{-1}$ for $\tau_{melt}$ values of 0.975 and 1.985, respectively, and the average interface speeds are 18 and 14 mm s$^{-1}$ (as shown later). From a typical morphology chart (p. 91 of Kurz and Fisher [1]) as shown in Fig. 2, the resulting microstructure will be fine corresponding to $\partial\bar{T}/\partial n|_I$ and $V_I$.

Figure 3 shows the solidification characteristics (i.e. $\theta_{bulk}$, $L/T$ and $\partial\bar{\theta}/\partial n|_I$) for a beam of 2.0 mm radius and $7.5 \times 10^8$ W m$^{-2}$ power density. The post-melting time is greater in this case—the superheat level is higher due to the higher power of the beam. The maximum values of $\partial\bar{T}/\partial n|_I$ are 867.0, 601.0 and 577.0 K mm$^{-1}$ for $\tau_{melt}$ values of 1.835, 5.255 and 7.735, respectively. The $\partial\bar{T}/\partial n|_I$ values for $\tau_{melt} = 5.255$ and 7.735 are nearly the same and this signifies that the fluid flow is near steady state for these melting times. As observed for the lower power case, the post-melting time is greater for the case of higher $\tau_{melt}$.

Figures 1 and 3 thus give a clear picture of the

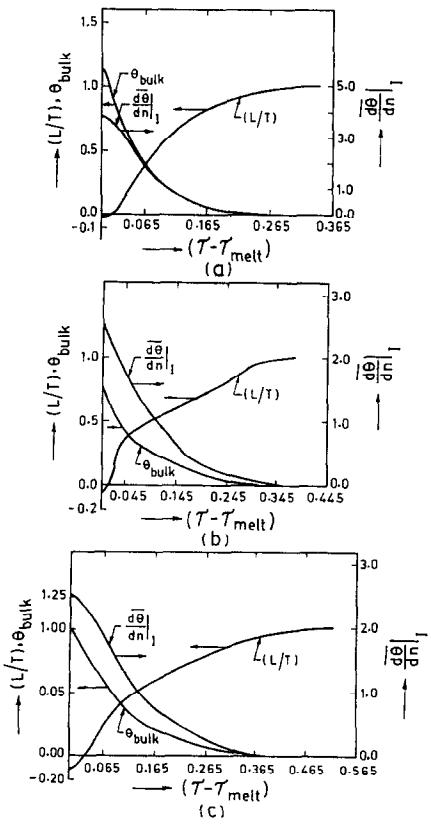


FIG. 3. The rate of change of the solidification characteristics, i.e. $(L/T)$, $\theta_{bulk}$ and $\partial\bar{\theta}/\partial n|_I$, for steel with a laser of $7.5 \times 10^8$ W m$^{-2}$ power density and 2.0 mm radius for various $\tau_{melt}$ values.

solidification after laser heating. From these studies, it is now possible to extract the rate of removal of total heat (both superheat and latent heat) at different times. While the rate of superheat removal gives the efficiency of the rapid solidification, the average temperature gradient at the solid/liquid interface provides a qualitative idea of the microstructure. These results will be utilized later to calculate the average cooling rate.

3.1.2. *Aluminium.* Figure 4 shows the variation of the solidification characteristics for a beam of 2 mm radius and $4.0 \times 10^8$ W m$^{-2}$ power density with different melting times ; $\tau_{melt} = 1.715$ and 1.875. Though the molten pool shape and the flow pattern are different for steel and aluminium, the variations of solidification characteristics with time are similar in nature. The fluid flow dies out very quickly during solidification and this results in a similar trend in the variation of the dimensionless average or global parameters like $\theta_{bulk}$, $(L/T)$ and $\partial\bar{\theta}/\partial n|_1$. The post-melting phenomenon is also seen for both cases of $\tau_{melt}$. The maximum average temperature gradients at the solid/liquid interface are 444.0 and 425.0 K mm$^{-1}$ for $\tau_{melt}$ values of 1.715 and 1.875, respectively. Due to the higher thermal conductivity of aluminium compared to steel, the temperature gradient at the solid/liquid interface is smaller in the case of aluminium. From the morphology chart [1], it can be seen (with the corresponding $V_1$ of 36 and 34 mm s$^{-1}$) that the microstructure will also be fine in this case.

The rate of removal of superheat $(L/T)$, the rate of decrease of melt superheat $(\theta_{bulk})$ and the average temperature gradient variation are similar for a beam of $7.5 \times 10^8$ W m$^{-2}$ power density for different $\tau_{melt}$ values (0.715, 0.995 and 1.725; see Fig. 5). The maximum average temperature gradients at the solid/liquid interface are 610.5, 525.0 and 407.0 K mm$^{-1}$ for melting times of 0.715, 0.995 and 1.725, respectively. The $\partial\bar{T}/\partial n|_1$ value for a $\tau_{melt}$ of 1.725 (= 407.0) is lower than that of the low power case with a $\tau_{melt}$ of 0.715 (= 425.0). This is again due to the better mixing with the more vigorous flow for the higher power beam than that for the lower power beam.

### 3.2. *Study of the pool characteristics*

3.2.1. *Steel.* Figure 6 shows the time variation of $r_{max}$, $z_{max}$ and $V_{max}$ of the liquid pool for a beam of 2.0 mm radius and $4 \times 10^8$ W m$^{-2}$ power density with melting times of 0.975 and 1.985, respectively. The rates of change of $r_{max}$ and $z_{max}$ with time show three distinct regions. Initially the rate of movement is slow which is due to post-melting. Beyond the post-melting when $(L/T)$ reaches 0.25, i.e. when $\Delta\tau$ is 0.022 and 0.038 for $\tau_{melt}$ values of 0.975 and 1.985, respectively (from Fig. 1), the rate of movement is faster; this can be clearly seen from Fig. 6(b). Once $(L/T)$ is greater than 0.9, i.e. when $\Delta\tau$ is more than 0.0625 and 0.0875 for $\tau_{melt}$ values of 0.975 and 1.985, respectively, the solidification proceeds at a very fast rate. This can be

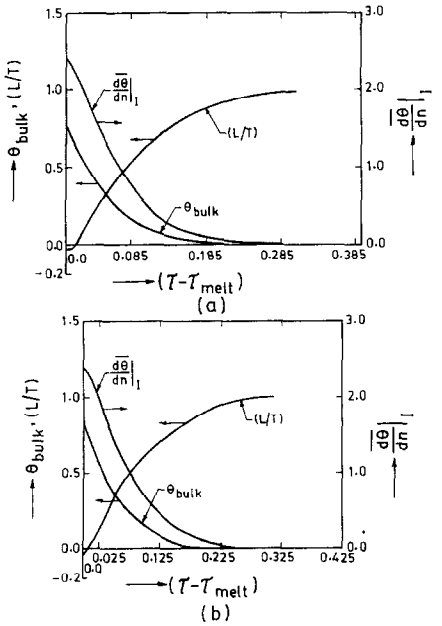


FIG. 4. The rate of change of the solidification characteristics, i.e. $(L/T)$, $\theta_{bulk}$ and $\partial\bar{\theta}/\partial n|_1$, for aluminium with a laser of $4.0 \times 10^8$ W m$^{-2}$ power density and 2.0 mm radius for various $\tau_{melt}$ values.

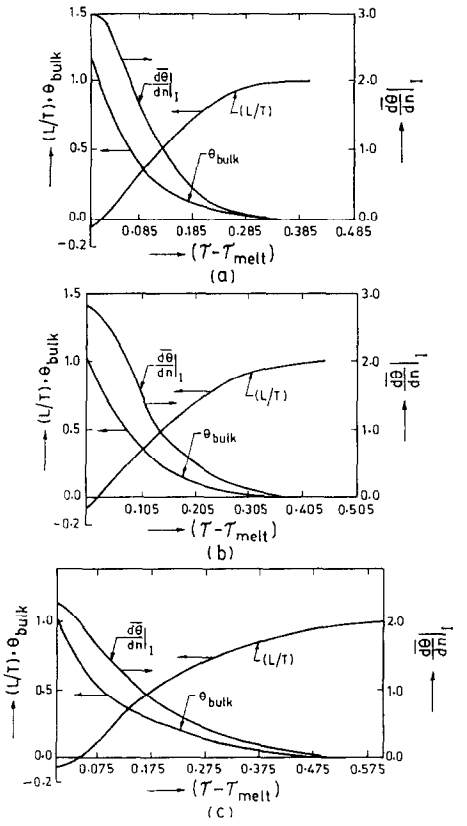


FIG. 5. The rate of change of the solidification characteristics, i.e. $(L/T)$, $\theta_{bulk}$ and $\partial\bar{\theta}/\partial n|_1$, for aluminium with a laser of $7.5 \times 10^8$ W m$^{-2}$ power density and 2.0 mm radius for various $\tau_{melt}$ values.

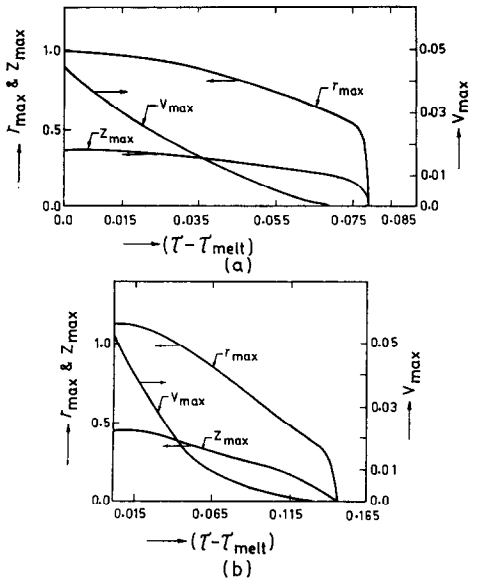


FIG. 6. The rate of change of pool characteristics, i.e. $r_{max}$, $z_{max}$ and $V_{max}$, with time for steel with a laser of $4.0 \times 10^8$ W m$^{-2}$ power density and 2.0 mm radius for various $\tau_{melt}$ values.

seen from the sudden drop in the $r_{max}$ and $z_{max}$ values during the final stage of solidification. Hence the total solidification process can be divided into three phases depending on the nature of the interface movement—slow, fast and very fast. The maximum velocity ($V_{max}$) of the flow, which occurs at the free surface, decreases at a fast rate during the initial time of solidification and then asymptotically approaches zero. The fast rate of decrease of the maximum velocity is already explained as being due to the reduction of the free surface temperature gradient by the flow. $V_{max}$ falls from 0.044 to 0.015 (i.e. 0.4 to 0.13 m s$^{-1}$) during the initial transient of solidification when $\tau_{melt}$ is 0.975. For $\tau_{melt} = 1.985$, $V_{max}$ decreases from 0.052 to 0.016 (i.e. 0.47 to 0.14 m s$^{-1}$) during this period of superheat release. This shows that the convective flow enhances the superheat release by better mixing and also reduces the driving force of the fluid flow during this period which is limited by superheat release.

The pool characteristics for the high power density beam (i.e. $q = 7.5 \times 10^8$ W m$^{-2}$) are shown in Fig. 7 with different melting times, i.e. 1.835, 5.255 and 7.735, respectively. The results are similar except for the initial period of slow solidification, which is longer in this case. Because of the higher power density, the amount of superheat to be removed is larger, which results in a longer period of slow solidification.

3.2.2. *Aluminium*. Figure 8 shows the variation of pool characteristics for a beam of 2.0 mm radius and $4 \times 10^8$ W m$^{-2}$ power density with different melting times, i.e. $\tau_{melt} = 1.715$ and 1.875, respectively. Like the solidification of steel, three distinct phases are also seen in this case depending on the rate of movement of $r_{max}$ and $z_{max}$. The maximum velocity ($V_{max}$) also decreases sharply during initial solidification and then

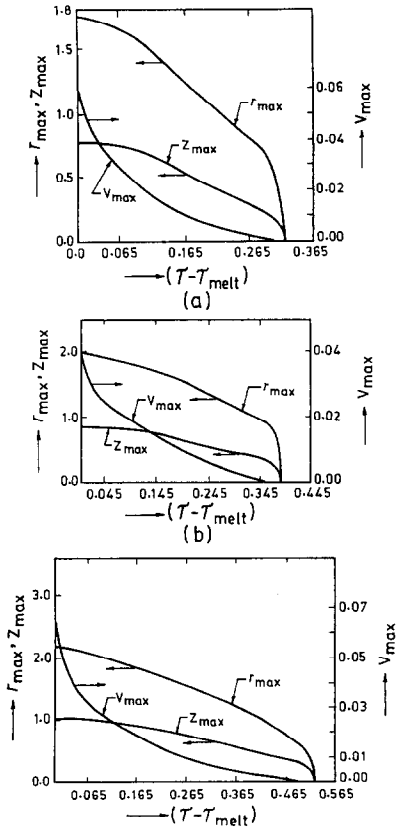


FIG. 7. The rate of change of pool characteristics, i.e. $r_{max}$, $z_{max}$ and $V_{max}$, with time for steel with a laser of $7.5 \times 10^8$ W m$^{-2}$ power density and 2.0 mm radius for various $\tau_{melt}$ values.

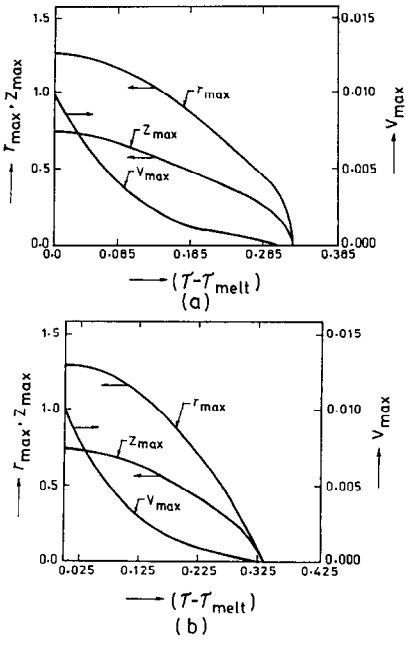


FIG. 8. The rate of change of pool characteristics, i.e. $r_{max}$, $z_{max}$ and $V_{max}$, with time for aluminium with a laser of $4.0 \times 10^8$ W m$^{-2}$ power density and 2.0 mm radius for various $\tau_{melt}$ values.

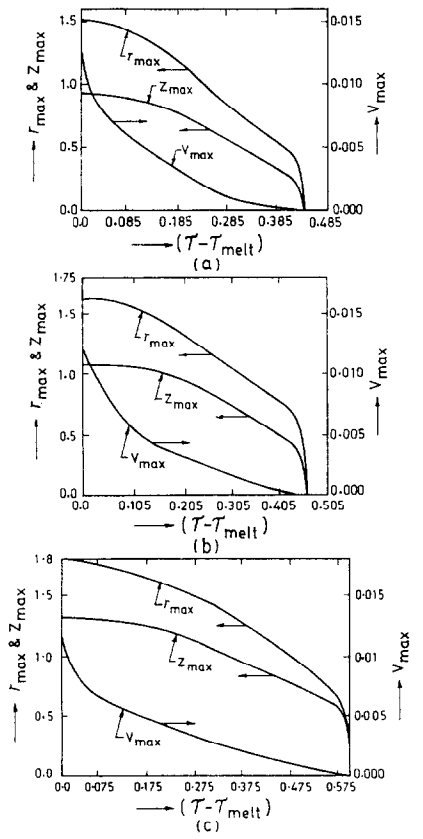


FIG. 9. The rate of change of pool characteristics, i.e. $r_{max}$, $z_{max}$ and $V_{max}$, with time for aluminium with a laser of $7.5 \times 10^8$ W $m^{-2}$ power density and 2.0 mm radius for various $\tau_{melt}$ values.

asymptotically approaches zero. The variations of pool characteristics for the case of higher power ($7.5 \times 10^8$ W $m^{-2}$) are also similar in nature (see Fig. 9).

### 3.3. *Characteristics of the latent heat release and the cooling rate*

The latent heat release compared to the total heat release ($L/T$) determines the efficiency of the heat extraction during solidification. The higher the value of ($L/T$) means the total heat to be removed is essentially latent heat. It is therefore interesting to compare various pool characteristics when ($L/T$) is 0.9, latent heat removal is the rate controlling parameter.

Table 1 shows the $\Delta\tau$ ($= \tau - \tau_{melt}$) for various $\tau_{melt}$ values to attain ($L/T$) of 0.9 for steel with $B_f = 28.94$ and 54.28. It can be seen that the higher the $\tau_{melt}$, the larger is the time to reach an ($L/T$) value of 0.9. This is obviously due to the higher superheat of the melt for higher $\tau_{melt}$, i.e. the laser is on for a longer duration. From the total solidification time given in Table 1, it can be seen that the superheat removal takes between 60 and 70% of the time taken for complete solidification (i.e. $\tau_{total\ solidification} - \tau_{melt}$). Once the superheat is removed, i.e. when $\tau_{melt}$ is greater than $\tau_{L/T=0.9}$, the solidification rate is faster when the essentially latent heat is removed. Hence, the order of the superheat should be as low as possible for rapid solidification. One interesting point to note is that the $\tau$ value for $V_{max}/V_{max,\tau_{melt}} = 0.9$ is almost equal to $\tau$ for ($L/T$) = 0.9 (see Table 1). The fluid flow will be present as long as there is superheat in the melt; only then will there be a surface temperature gradient (although of small order) to drive the flow. Hence, there is a direct relationship between the rate of decay of flow and the rate of superheat removal. The trend of the results is the same for aluminium, as can be seen from Table 2.

Tables 3 and 4 show the melt width ($r_{max}$) and depth ($z_{max}$) at time $\tau_{L/T=0.9}$ with different $\tau_{melt}$ values for steel and aluminium, respectively. $r_{max}$ and $z_{max}$ are seen to be higher at $\tau_{L/T=0.9}$ for higher $\tau_{melt}$, which is again due to the higher superheat level. Because of the higher *Ste*, the percentage movement for steel is higher than that for aluminium. By comparing percentage movement of $r_{max}$ and $z_{max}$ of all the cases, it can be seen that the percentage of $z_{max}$ is always higher than that for $r_{max}$ except for the case of aluminium with higher power (i.e. $B_f = 37.47$). Due to the stronger primary cell, there is better mixing at the top than at the bottom during this period and, as a result, the rate of loss of superheat is higher at the top than that of latent heat. This leads to relatively slower movement of the solid/liquid interface at the top during this period. In the case of aluminium with higher power density, there also exists a stronger secondary cell [9], which enhances superheat release at the bottom. As a result, the interface movement is relatively slow at the bottom, unlike all the other cases.

Table 1. Differential times, i.e. $\Delta\tau = (\tau - \tau_{melt})$, for ($L/T$) = 0.9, total solidification and $V_{max}/V_{max,\tau_{melt}} = 0.9$ for steel with $R_\sigma = 23040.0$ and $Ma = 1806.0$

| $B_f$ | $\tau_{melt}$ | $\Delta\tau$ for ($L/T$) = 0.9 ($\Delta\tau_1$) | $\Delta\tau$ for total solidification ($\Delta\tau_2$) | $\frac{\Delta\tau_1}{\Delta\tau_2} \times 100$ | $\Delta\tau$ for $\frac{V_{max}}{V_{max,\tau_{melt}}} = 0.9$ |
|---|---|---|---|---|---|
| 28.94 | 0.975 | 0.06 | 0.089 | 66.7 | 0.056 |
| | 1.985 | 0.09 | 0.140 | 65.0 | 0.087 |
| 54.28 | 1.835 | 0.19 | 0.32 | 59.4 | 0.212 |
| | 5.255 | 0.28 | 0.41 | 68.3 | 0.286 |
| | 7.735 | 0.33 | 0.47 | 70.2 | 0.321 |

Table 2. Differential times, i.e. $\Delta\tau = (\tau - \tau_{melt})$, for $(L/T) = 0.9$, total solidification and $V_{max}/V_{max,\tau_{melt}} = 0.9$ for aluminium with $R_\sigma = 701\,000.0$ and $Ma = 6912.0$

| $B_f$ | $\tau_{melt}$ | $\Delta\tau$ for $(L/T) = 0.9$ $(\Delta\tau_1)$ | $\Delta\tau$ for total solidification $(\Delta\tau_2)$ | $\frac{\Delta\tau_1}{\Delta\tau_2} \times 100$ | $\Delta\tau$ for $\frac{V_{max}}{V_{max,\tau_{melt}}} = 0.9$ |
|---|---|---|---|---|---|
| 20.0 | 1.715 | 0.19 | 0.32 | 59.3 | 0.210 |
| | 1.875 | 0.20 | 0.33 | 61.0 | 0.213 |
| 37.47 | 0.715 | 0.25 | 0.44 | 56.8 | 0.276 |
| | 0.995 | 0.31 | 0.46 | 67.4 | 0.321 |
| | 1.235 | 0.37 | 0.54 | 68.5 | 0.418 |
| | 1.725 | 0.42 | 0.60 | 70.0 | 0.447 |

Table 3. Melt width ($r_{max}$) and depth ($z_{max}$) at time when $(L/T) = 0.9$ for steel with $R_\sigma = 23\,040.0$ and $Ma = 1806.0$

| $B_f$ | $\tau$ for $(L/T) = 0.9$ | $r_{max}$ | $z_{max}$ | $\frac{(r_{max,\tau_{melt}} - r_{max})}{r_{max,\tau_{melt}}} \times 100$ | $\frac{(z_{max,\tau_{melt}} - z_{max})}{z_{max,\tau_{melt}}} \times 100$ |
|---|---|---|---|---|---|
| 28.94 | 1.044 | 0.612 | 0.20 | 38.75 | 46.70 |
| | 2.073 | 0.687 | 0.25 | 38.89 | 44.40 |
| 54.28 | 2.023 | 1.106 | 0.437 | 36.30 | 43.54 |
| | 5.534 | 1.225 | 0.475 | 38.75 | 44.90 |
| | 8.069 | 1.550 | 0.725 | 29.8 | 29.3 |

Table 4. Melt width ($r_{max}$) and depth ($z_{max}$) at time when $(L/T) = 0.9$ for aluminium with $R_\sigma = 701\,000.0$ and $Ma = 6912.0$

| $B_f$ | $\tau$ for $(L/T) = 0.9$ | $r_{max}$ | $z_{max}$ | $\frac{(r_{max,\tau_{melt}} - r_{max})}{r_{max,\tau_{melt}}} \times 100$ | $\frac{(z_{max,\tau_{melt}} - z_{max})}{z_{max,\tau_{melt}}} \times 100$ |
|---|---|---|---|---|---|
| 20.0 | 1.91 | 0.825 | 0.476 | 35.30 | 36.60 |
| | 2.07 | 0.850 | 0.487 | 34.10 | 37.00 |
| 37.47 | 0.967 | 0.963 | 0.644 | 36.24 | 31.30 |
| | 1.368 | 1.019 | 0.712 | 37.30 | 33.70 |
| | 1.575 | 1.137 | 0.819 | 35.00 | 30.00 |
| | 2.139 | 1.260 | 0.906 | 34.00 | 31.00 |

3.3.1. *Cooling rate.* The average solid/liquid interface velocity between $\tau_{melt}$ and $\tau_{L/T=0.9}$ is calculated using Tables 1–4 as follows:

at the top

$$\bar{V}_1 = \frac{(r_{max,\tau_{melt}} - r_{max,\tau_{(L/T=0.9)}})}{(\tau_{melt} - \tau_{(L/T=0.9)})};$$

at the bottom

$$\bar{V}_1 = \frac{(z_{max,\tau_{melt}} - z_{max,\tau_{(L/T=0.9)}})}{(\tau_{melt} - \tau_{(L/T=0.9)})}.$$

The average temperature gradient at the solid/liquid interface is calculated from Figs. 1 and 2–5 as follows:

$$\left.\frac{\partial\bar{\theta}}{\partial n}\right|_1 = \frac{(\partial\bar{\theta}/\partial n|_{1,\tau_{melt}} + \partial\bar{\theta}/\partial n|_{1,\tau_{(L/T=0.9)}})}{2.0}.$$

Using $\bar{V}_1$ and $\partial\bar{\theta}/\partial n|_1$, the average cooling rate $|\dot{\theta}|$ is calculated as follows:

$$|\dot{\theta}| = \bar{V}_1 \left.\frac{\partial\bar{\theta}}{\partial n}\right|_1.$$

The non-dimensional cooling rate, $|\dot{\theta}|$, is transformed into dimensional form as follows:

$$|\dot{T}| = \frac{\lambda\alpha}{C_p r_0^2}|\dot{\theta}|$$

$$= 1160.0\,|\dot{\theta}| \quad \text{for steel}$$

$$= 3474.0\,|\dot{\theta}| \quad \text{for aluminium.}$$

Tables 5 and 6 provide $V_1$, $\partial\bar{\theta}/\partial n|_1$ and $|\dot{\theta}|$ averaged between $\tau_{melt}$ and $\tau_{L/T=0.9}$ with different $\tau_{melt}$ and $B_f$ values for steel and aluminium, respectively. It can be seen that the average cooling rate is between $10^4$ and $10^5$ K s$^{-1}$. From Fig. 2, it can be seen that the scale of microstructure will be very fine, thereby ensuring improved surface properties. The average cooling rate at the top surface is always seen to be higher than

Table 5. Average interface velocity ($\bar{V}_I$), solid/liquid temperature gradient ($\partial\bar{\theta}/\partial n|_I$) and cooling rate ($|\dot{\theta}|$) during $\tau_{melt}$ and $\tau_{L/T=0.9}$ for steel with $R_\sigma = 23040.0$ and $Ma = 1806.0$

| | | $\bar{V}_I$ | | | $\lvert\dot{\theta}\rvert$ | | $\lvert\dot{T}\rvert$ (K s$^{-1}$ × 10$^5$) | |
|---|---|---|---|---|---|---|---|---|
| $B_f$ | $\tau_{melt}$ | Top | Bottom | $\partial\bar{\theta}/\partial n\|_I$ | Top | Bottom | Top | Bottom |
| 28.94 | 0.975 | 4.50 | 2.80 | 2.83 | 12.73 | 7.90 | 1.48 | 0.92 |
| | 1.985 | 3.50 | 2.19 | 2.375 | 8.31 | 5.20 | 0.96 | 0.60 |
| 54.28 | 1.835 | 3.37 | 1.80 | 2.970 | 10.0 | 5.35 | 1.16 | 0.62 |
| | 5.255 | 2.77 | 1.39 | 1.300 | 3.6 | 1.80 | 0.42 | 0.21 |
| | 7.735 | 1.91 | 0.99 | 1.275 | 2.4 | 1.26 | 0.28 | 0.15 |

Table 6. Average interface velocity ($\bar{V}_I$), solid/liquid temperature gradient ($\partial\bar{\theta}/\partial n|_I$) and cooling rate ($|\dot{\theta}|$) during $\tau_{melt}$ and $\tau_{L/T=0.9}$ for aluminium with $R_\sigma = 701000.0$ and $Ma = 6912.0$

| | | $\bar{V}_I$ | | | $\lvert\dot{\theta}\rvert$ | | $\lvert\dot{T}\rvert$ (K s$^{-1}$ × 10$^5$) | |
|---|---|---|---|---|---|---|---|---|
| $B_f$ | $\tau_{melt}$ | Top | Bottom | $\partial\bar{\theta}/\partial n\|_I$ | Top | Bottom | Top | Bottom |
| 20.0 | 1.715 | 2.34 | 1.46 | 1.25 | 2.93 | 1.83 | 1.02 | 0.63 |
| | 1.875 | 2.20 | 1.44 | 1.23 | 2.70 | 1.77 | 0.94 | 0.61 |
| 37.47 | 0.715 | 2.17 | 1.16 | 1.57 | 3.40 | 1.83 | 1.18 | 0.63 |
| | 0.995 | 1.96 | 1.17 | 1.47 | 2.88 | 1.72 | 0.99 | 0.59 |
| | 1.235 | 1.67 | 1.07 | 1.23 | 2.05 | 1.30 | 0.71 | 0.45 |
| | 1.725 | 1.50 | 1.01 | 1.20 | 1.80 | 1.21 | 0.62 | 0.42 |

Note that the cooling rates at the top and bottom of the molten pool are calculated based on the rate of movement of $r_{max}$ and $z_{max}$, respectively.

that at the bottom of the pool, i.e. along the line of symmetry. This predicted result is consistent with the experimental observation where a finer microstructure is seen at the top edge than at the bottom [5, 10]. For the same power density and radius of the beam, the average cooling rate decreases with the increase of $\tau_{melt}$. For higher $\tau_{melt}$, the interface moves relatively slowly due to higher superheat and the order of $|\dot{\theta}|$ reduces due to better mixing of the molten pool. As a result, the cooling rate decreases.

Hence, the beam specifications should be selected in such a way that $\tau_{melt}$ (which is also known as the interaction time) is a minimum to attain a certain depth. This criterion is used to obtain a higher cooling rate which, in turn, ensures a finer microstructure and improved properties.

## 4. CONCLUSIONS

The conclusions of this work can be summarized as follows.

(i) Even after the heat source is removed, there is a small amount of melting (i.e. post-melting) which takes place due to the superheat of the melt, depending on the melting time.

(ii) $\theta_{bulk}$ and $\partial\bar{\theta}/\partial n|_I$ fall very quickly during the initial period of solidification when $(L/T)$ approaches unity, and the solidification beyond this point is controlled by latent heat removal.

(iii) The efficiency of the rapid solidification for various cases can be determined from the variation of the solidification characteristic graphs developed here. These graphs are utilized to calculate the interface speed, solid/liquid temperature gradient and the cooling rate.

(iv) By comparison with the morphology chart, the maximum average temperature gradient at the solid/liquid interface and the cooling rate show that the resultant microstructure will be fine.

(v) From the variation of $r_{max}$ and $z_{max}$ with time, three distinct phases of solidification are noted depending on the front movement—slow, fast and very fast. These three phases are dependent on the nature of heat removal, i.e. superheat, (superheat + latent heat) and latent heat.

(vi) From the predicted maximum velocity variation with time, it is found that the flow dies out mainly in the period of superheat removal.

(vii) The cooling rates for steel and aluminium are calculated and shown to be between $10^4$ and $10^5$ K s$^{-1}$. Due to the higher superheat level, the cooling rate decreases with the increase of interaction time.

(viii) The local cooling rate at the top of the pool is always higher than that at the bottom. As a result, the microstructure at the top of the pool will always be finer than that at the bottom.

*Acknowledgements*—The authors thank Prof. E. C. Subbarao, Director, Tata Research Development and Design Centre, Pune, for his encouragement. This work was supported by a project from Defence Research and Development Organization, New Delhi.

## REFERENCES

1. B. Kurz and D. J. Fisher, *Fundamentals of Solidification*. Trans. Tech., Switzerland (1986).

2. S. C. Hsu, S. Chakraborty and R. Mehrabian, Rapid melting and solidification of a surface layer, *Metall. Trans.* **9B,** 221–229 (1978).
3. S. C. Hsu, S. Kuo and R. Mehrabian, Rapid melting and solidification due to a stationary heat flux, *Metall. Trans.* **11B,** 24–28 (1980).
4. S. Kou, S. C. Hsu and R. Mehrabian, Rapid melting and solidification due to a moving heat flux, *Metall. Trans.* **12B,** 33–45 (1981).
5. J. A. Sekhar, S. Kou and R. Mehrabian, Heat flow model for surface melting and solidification of an alloy, *Metall. Trans.* **14A,** 1169–1177 (1984).
6. K. V. Ramarao and J. A. Sekhar, Unsteady rapid solidification with a moving heat source, *Acta Metall.* **35,** 81–87 (1986).
7. A. Paul and T. Debroy, Free surface flow and heat transfer in conduction mode laser welding, *Metall. Trans.* **19B,** 851–858 (1988).
8. G. M. Oreper, J. Szekeley and T. Eager, The role of transient convection in the melting and solidification in the arc weld pools, *Metall. Trans.* **17B,** 735–744 (1986).
9. B. Basu and A. W. Date, Rapid solidification following laser melting of pure metals—I. Study of flow field and role of convection, *Int. J. Heat Mass Transfer* **35,** 1049–1058 (1992).
10. C. Chan, J. Mazumder and M. M. Chen, A two dimensional transient model for convection in laser melted pool, *Metall. Trans.* **15A,** 2175–2184 (1984).

## SOLIDIFICATION RAPIDE APRES FUSION LASER DE METAUX PURS—II. ETUDE DES CARACTERISTIQUES ET DU BAIN DE LA SOLIDIFICATION

**Résumé**—Divers paramètres de la solidification comme le gradient de température solide/liquide, vitesse de refroidissement, nature de la libération de la chaleur latente et caractéristiques du bain (vitesse de changement de largeur, de profondeur et de vitesse maxi) sont étudiés pour une rapide solidification successive à une fusion laser d'aluminium et d'acier. Pour un laser de rayon fixé (2,0 mm), les études sont conduites avec différentes densités de puissance entre $10^8$ et $10^9$ W m$^{-2}$. Il y a fusion ("post-fusion") même après arrêt de laser et l'importance est liée à la surchauffe du bain. A partir du gradient de température à l'interface solide/liquide et de la vitesse de refroidissement, on montre que la microstructure du matériau solidifié est très fine et qu'elle est toujours plus fine au sommet du bain qu'à la base.

## SCHNELLE VERFESTIGUNG NACH DEM AUFSCHMELZEN REINER METALLE MITTELS LASER—II. UNTERSUCHUNG DES SCHMELZBADES UND SEINER VERFESTIGUNG

**Zusammenfassung**—Es wird der Einfluß einer Reihe von Parametern auf die plötzliche Erstarrung eines Schmelzbades aus Aluminium und Stahl untersucht, das zuvor mittels Laser erschmolzen worden war: Temperaturgradient in Feststoff und Flüssigkeit, Abkühlrate, Art der Freisetzung der Erstarrungswärme, zeitliche Änderung von Breite und Tiefe des Bades sowie maximale Geschwindigkeit im Bad. Die Untersuchung wurde bei festgehaltenem Radius des Laserstrahls (2,0 mm) und verschiedenen Leistungsdichten zwischen $10^8$ und $10^9$ W m$^{-2}$ durchgeführt. Sogar nach Abschalten des Lasers tritt noch Schmelzen (nämlich sogenanntes Nach-Schmelzen) auf, was vom Ausmaß der Überhitzung des Bades abhängt. Abhängig vom Temperaturgradienten an der Fest-/Flüssig-Phasengrenze und der Abkülungsrate zeigt sich, daß die Mikrostruktur des erstarrten Materials sehr fein ist, und daß die Mikrostruktur im oberen Teil des Bades immer feiner ist also im unteren Teil.

## БЫСТРОЕ ЗАТВЕРДЕВАНИЕ ЧИСТЫХ МЕТАЛЛОВ ПОСЛЕ ЛАЗЕРНОЙ ПЛАВКИ—II. ИССЛЕДОВАНИЕ ХАРАКТЕРИСТИК ОБЪЕМА РАСПЛАВА И ПРОЦЕССА ЗАТВЕРДЕВАНИЯ

**Аннотация**—Исследуются различные параметры процесса затвердевания, включая градиент температур твердой и жидкой фаз, скорость охлаждения, механизм скрытого тепловыделения, а также такие характеристики объема расплава, как интенсивность изменения его ширины, глубины и максимальная скорость при быстром затвердевании после лазерой плавки алюминия и стали. В случае постоянного радиуса лазерного пучка (составляющего 2,0 мм) исследования проводятся с использованием различных величин плотности мощности лазера, изменяющихся в диапазоне $10^8$–$10^9$ Вт. м$^{-2}$. Плавление (т.е. "последующее плавление") происходит даже после удаления лазера и определяется перегревом объема расплава. Исследование градиента температур на границе раздела твердое тело—жидкость показывает, что микроструктура затвердевающего материала является весьма мелкой и в верхней части объема расплава она всегда более мелкая, чем в нижней.